Experimental Neurology 350 (2022) 113978

Contents lists available at ScienceDirect

Experimental Neurology

journal homepage: www.elsevier.com/locate/yexnr

Research paper

Deep brain stimulation electrode modeling in rats

Andrea Andree [a,*,1], Ningfei Li [b,1], Konstantin Butenko [a,b], Maria Kober [c], Jia Zhi Chen [d], Takahiro Higuchi [e], Mareike Fauser [c], Alexander Storch [c,f,g], Chi Wang Ip [d], Andrea A. Kühn [b], Andreas Horn [b,i,j,1], Ursula van Rienen [a,g,h,*,1]

[a] Institute of General Electrical Engineering, University of Rostock, Albert-Einstein-Straße 2, 18059 Rostock, Germany
[b] Charité – Universitätsmedizin Berlin, corporate member of Freie Universität Berlin and Humboldt-Universität zu Berlin, Movement Disorders and Neuromodulation Unit, Department of Neurology, Charitéplatz 1, 10117 Berlin, Germany
[c] Department of Neurology, University of Rostock, Gehlsheimer Straße 20, 18147 Rostock, Germany
[d] Department of Neurology, University Hospital of Würzburg, Josef-Schneider-Straße 11, 97080 Würzburg, Germany
[e] Department of Nuclear Medicine and Comprehensive Heart Failure Center, University Hospital of Würzburg, Oberdürrbacher Straße 6, 97080 Würzburg, Germany
[f] German Centre for Neurodegenerative Diseases (DZNE) Rostock/Greifswald, Gehlsheimer Straße 20, 18147 Rostock, Germany
[g] Department Ageing of Individuals and Society, University of Rostock, Gehlsheimer Straße 20, 18147 Rostock, Germany
[h] Department Life, Light & Matter, University of Rostock, Albert-Einstein-Straße 25, 18059 Rostock, Germany
[i] Center for Brain Circuit Therapeutics, Department of Neurology Brigham & Women's Hospital, Harvard Medical School, Boston, United States
[j] MAMGH Neurosurgery & Center for Neurotechnology and Neurorecovery (CNTR) at MGH Neurology, Massachusetts General Hospital, Harvard Medical School, Boston, MA, United States

ARTICLE INFO

Keywords:
Deep brain stimulation
Parkinson's disease
Animal models
Rat
Rodent
Neuroimaging
Open-source
Research software

ABSTRACT

Deep Brain Stimulation (DBS) is an efficacious treatment option for an increasing range of brain disorders. To enhance our knowledge about the mechanisms of action of DBS and to probe novel targets, basic research in animal models with DBS is an essential research base. Beyond nonhuman primate, pig, and mouse models, the rat is a widely used animal model for probing DBS effects in basic research. Reconstructing DBS electrode placement after surgery is crucial to associate observed effects with modulating a specific target structure. *Post-mortem* histology is a commonly used method for reconstructing the electrode location. In humans, however, neuroimaging-based electrode localizations have become established.

For this reason, we adapt the open-source software pipeline Lead-DBS for DBS electrode localizations from humans to the rat model. We validate our localization results by inter-rater concordance and a comparison with the conventional histological method. Finally, using the open-source software pipeline OSS-DBS, we demonstrate the subject-specific simulation of the VTA and the activation of axon models aligned to pathways representing neuronal fibers, also known as the pathway activation model. Both activation models yield a characterization of the impact of DBS on the target area.

Our results suggest that the proposed neuroimaging-based method can precisely localize DBS electrode placements that are essentially rater-independent and yield results comparable to the histological gold standard. The advantages of neuroimaging-based electrode localizations are the possibility of acquiring them *in vivo* and combining electrode reconstructions with advanced imaging metrics, such as those obtained from diffusion or functional magnetic resonance imaging (MRI). This paper introduces a freely available open-source pipeline for DBS electrode reconstructions in rats. The presented initial validation results are promising.

* Corresponding authors.
E-mail addresses: andrea.andree@uni-rostock.de (A. Andree), ningfei.li@charite.de (N. Li), konstantin.butenko@uni-rostock.de (K. Butenko), Maria.Kober@med.uni-rostock.de (M. Kober), chen_j@ukw.de (J.Z. Chen), higuchi_t@ukw.de (T. Higuchi), Mareike.Fauser@med.uni-rostock.de (M. Fauser), Alexander.Storch@med.uni-rostock.de (A. Storch), ip_c@ukw.de (C.W. Ip), andrea.kuehn@charite.de (A.A. Kühn), andreas.horn@charite.de (A. Horn), ursula.van-rienen@uni-rostock.de (U. van Rienen).
[1] Authors contributed equally.

https://doi.org/10.1016/j.expneurol.2022.113978
Received 17 June 2021; Received in revised form 13 November 2021; Accepted 6 January 2022
Available online 11 January 2022

1. Introduction

Deep brain stimulation (DBS) is an efficacious treatment option for various brain disorders and is an established treatment for movement disorders such as Parkinson's Disease, dystonia, or essential tremor (Deuschl et al., 2006; Kupsch et al., 2006). DBS opens up a window to record electrophysiological data from the living human brain (Kühn et al., 2004; Neumann and Kühn, 2017). Also, it has led to tremendous insights into the pathophysiology of multiple diseases (Krauss et al., 2020; Vedam-Mai et al., 2021). Nevertheless, for ethical reasons, many open scientific questions in humans cannot be resolved.

Animal models, such as the 6-hydroxy-dopamine rodent and 1-methyl-4-phenyl-1,2,3,6-tetrahydropyridine macaque Parkinson's disease models, have promoted our understanding by permitting recordings of local field potentials in healthy *vs.* Parkinsonian states and can be deliberately controlled (Bergman, 2021; Sanders and Jaeger, 2016). Additional benefits of animal models can, among other things, be seen in (i) the possibility to record from multiple regions of the brain in parallel and (ii) the accurate *post-mortem* histological localization of stimulation electrodes using microscopy. The latter can involve specific histological staining methods that further support the research question at hand. Here, we focus on precisely this latter point, namely electrode localization. Ensuring accurate electrode placements in the targeted region is a central and crucial point for almost all DBS research questions (Treu et al., 2020). In human and animal studies alike, the inaccurate placement of electrodes in another region that researchers assumed may lead to drastic misinterpretation of scientific results (Horn, 2019).

For the application in humans, neuroimaging for DBS electrode localizations has been developed since the earlier 2000s (D'Haese et al., 2012; Miocinovic et al., 2007; Yelnik et al., 2003). In recent years, the methodology has become increasingly accurate (Horn, 2019; Horn et al., 2019a; Krauss et al., 2020). Thus, reproducible insights across groups (Akram et al., 2017; Bot et al., 2018; Caire et al., 2013; Horn, 2019), transferrable across patients, cohorts, and DBS centers (Al-Fatly et al., 2019; Horn et al., 2017; Irmen et al., 2020; Li et al., 2021, Li et al., 2020) could be achieved.

While histological confirmation of DBS electrode placement in animal studies is considered the gold standard in the field (Borg et al., 2015; Király et al., 2020; Masís et al., 2018; Rangarajan et al., 2016), the approach suffers from several disadvantages:

First, histology has some disadvantages regardless of elaborated staining possibilities: It primarily leads to two-dimensional datasets that are not straightforward to reconstruct in three dimensions (*e.g.*, for fusion with digital 3D atlases) (Alho et al., 2017; Amunts et al., 2013). Problems such as the "straight banana problem" (Casero et al., 2017) will occur, and even in two-dimensional planes, shearing and straining of the tissue could lead to imprecisions of dimensions along the imaging plane (Alho et al., 2017). Conventionally, the target accuracy is assessed by aligning histological sections with a stereotactic atlas (Paxinos and Watson, 2007). In this manner, the localization of the electrode's tip is feasible. Still, a 3D reconstruction of the trajectory of the lead and objective quantification of the planned trajectory is not easy to implement.

Second, combining electrode localizations with advanced imaging modalities, such as diffusion-weighted magnetic resonance imaging (dMRI) or functional MRI, enables answering novel scientific questions (Horn et al., 2019b; Horn and Fox, 2020). The latter is not straightforward when relying on histological localization.

Since the diameter of the electrodes is very small related to their length (100–200 μm relative to 10 mm, respectively), the practical problem is that they may easily bend during implantation unless using a guide cannula. Therefore, without a guide cannula, the trajectory may deviate from the planned path. Thus, third, electrodes that are not implanted orthogonally to the processed tissue sections might not be represented well and will complicate creating accurate 3D models of the electrode's trajectory (Borg et al., 2015; Rangarajan et al., 2016). Thus, an interesting concept both for histology and MRI-based localization is the use of a guiding cannula, which can be localized in the MRI even before inserting electrodes and prevent bending of electrodes (Apetz et al., 2019).

Fourth, metal electrodes are considerably harder than the surrounding tissue. The electrodes cannot remain in the brain when the histological sections are generated. It may lead to tissue damage when extracting the electrode (Borg et al., 2015).

Fifth, this method requires the sacrifice of animals. Long-term studies lead to more animals being tested and sacrificed. Additionally, when behavioral studies are conducted, an end-point histological verification of off-target and on-target subjects might lead to loss of time and resources due to dropouts in animals for *post-mortem* histology (Rangarajan et al., 2016). *Post-mortem* histological verification of the precise localization of the electrode tip requires specific tissue processing such as paraformaldehyde (PFA) fixation and standardized tissue sectioning to obtain optimal morphological and anatomical structures. In addition, scientific questions other than electrode localization most often demand other neurobiological methods than histology. For technical reasons, a simultaneous investigation combining histological tip localization with additional methods (quantitative polymerase chain reaction and western blot) is nearly impossible. The latter underlines the advantage of accurately localizing the electrode using a technique independent of tissue processing.

Abbreviations

DBS	deep brain stimulation
MRI	magnetic resonance imaging
dMRI	diffusion-weighted magnetic resonance imaging
VTA	volume of tissue activated
PAM	pathway activation model
PFA	paraformaldehyde
WI(Han)	Wistar (Han)
SD	Sprague Dawley
P&W atlas	atlas based on (Paxinos and Watson, 2007)
WHS atlas	atlas in Waxholm space
RMSE	root mean square error
CSF	cerebrospinal fluid
STN	subthalamic nucleus (= STh in (Paxinos and Watson, 2007))
Std Dev	standard deviation

Abbreviations in the notation of (Paxinos and Watson, 2007)

CA1/CA2/CA3	field CA1/CA2/CA3 of the hippocampus
EP	entopeduncular nucleus
LV	lateral ventricle
(D)3 V	(dorsal) 3rd ventricle
ac	anterior commissure
cc	corpus callosum
cp	cerebral peduncle
ic	internal capsule
mt	mammillothalamic tract
opt	optic tract
sox	supraoptic tract

Furthermore, the exact localization of the electrodes plays an important role when modeling DBS *in silico to estimate, e.g., the volume* of tissue activated (VTA).

The VTA *is either an* approximation based on the electric field distribution caused by DBS, as described by Åström et al. (2012). Another approach is to estimate the VTA based on the firing activity of axon cable models placed at increasing distances to the electrode (Butson and McIntyre, 2005; McIntyre et al., 2002). The third approach is to characterize the activation of axon cable models placed along anatomically plausible pathways. The latter is known as the pathway activation model (PAM) (Gunalan et al., 2017; Howell and McIntyre, 2016). We employed the recently published open-source toolbox OSS-DBS (https://github.com/SFB-ELAINE/OSS-DBS; (Butenko et al., 2020)) to characterize the brain tissue activated due to DBS. OSS-DBS is a Python-controlled toolbox creating a volume conductor model of the rat brain, including heterogeneous and anisotropic dielectric tissue properties. The importance of using frequency-dependent (Butson and McIntyre, 2005; Grant and Lowery, 2010), heterogeneous (Howell and McIntyre, 2017), and anisotropic (Åström et al., 2012; Schmidt and van Rienen, 2012) models have been described in detail in human *in silico* models. Hence, for creating exact volume conductor models of a rat brain, segmented MRI (separating white, gray matter, and cerebrospinal fluid) is vital to include the heterogeneity of the brain tissue. Also, co-registered diffusion tensors derived from diffusion MRI (dMRI) are essential to assessing the anisotropic nature, especially of white matter fiber tracts. This methodology is described in the chapter *Pipeline Adaptation: Lead-DBS for the Rat*. The creation of volume conductor models for DBS in rat brains is still an evolving field (Böhme and van Rienen, 2016; Butenko et al., 2020; Schmidt et al., 2018; Sridhar et al., 2019). To visualize and model comparably small target structures for DBS in the rat, such as the subthalamic nucleus (STN), relatively high imaging resolution is needed. In rats, the lens-shaped STN has a size of 0.8 ± 0.1 mm^3, which is about 300 times smaller than the human STN (Hardman et al., 2002). In addition to high imaging resolution, the exact localization of the electrode is of great importance to estimate the effects of activated neuronal fibers, especially considering the tiny size of the target structures of DBS in rats.

Borg et al. (2015) introduced a "multistep registration procedure based on the skull." This procedure could produce good co-registration results between individual computer tomography (CT) scans and high-resolution MRI atlas (Johnson et al., 2012). While MRI enables clear visualizing of soft tissue, CT scans can be acquired much quicker, likely reducing animal movement artifacts and stress.

DBS electrodes cause artifacts in MRI and CT images as an undesired obstacle: Bright streaks in the tissue encasing the electrode's lead are associated with beam hardening and scatter effects caused by metals in CT scans. These artifacts can be compensated by feasible scanning parameters optimized for the respective CT scanner used.

The artifacts and side effects (electrode movement in extreme cases) in MRI are not negligible. While Borg et al. (2015) presented an approach for *ex vivo* imaging, Rangarajan et al. (2016) introduced a multi-modal pipeline for *in vivo* electrode localization in rats based on preoperative and postoperative CTs and MRIs, which they also normalized to the high-resolution MRI atlas (Johnson et al., 2012). Inspired by these first approaches, we adapted them to the requirements of DBS rat models with chronic electrodes to avoid beam hardening effects due to the implanted electrode. In addition, we include *in silico* modeling to estimate the VTA and create pathway activation models.

This paper probes the first steps of transferring a widespread and elaborate electrode localization pipeline for humans, Lead-DBS (www.lead-dbs.org; (Horn and Kühn, 2015)), to the rat model. We first establish a set of imaging parameters using CT in eleven animals from two centers. We then adjust the code developed for human research to the rat model and evaluate the usability and reliability of the software by comparing electrode localization of a group of animals from two centers as carried out by two of the software developers (user AA and NL). In a subset of animals for which histological workup is available, we compare the results of the two users to stereotactic P&W atlas coordinates estimated by anatomical experts (expert MK and CI). Previously, postoperative *ex vivo* (Borg et al., 2015) and preoperative and postoperative *in vivo* localization studies (Rangarajan et al., 2016) were developed and evaluated using the high-resolution MRI atlas (Johnson et al., 2012). In this study, we compare the localization performed in two rat strains (Wistar-Han (WI (Han)) and Sprague Dawley (SD)) using the Waxholm Space (WHS) atlas (Papp et al., 2014) by aligning postoperative CT images with the atlas space. Therefore, we visually compared MRI-based and histology-based P&W atlas coordinates as a next objective. We combine Lead-DBS-based electrode localizations with field computations in OSS-DBS (Butenko et al., 2020) to assess the effect of DBS in rats (quantified by the size and shape of the VTA as well as axonal activation patterns during pathway activation modeling). A monopolar DBS electrode, implanted in a WI (Han) rat, serves as an example.

The current study is mainly methodological and consists of an adaptation of Lead-DBS and OSS-DBS for rats. Both simulation pipelines are made openly available, and subsequent studies may further assess the utility of our tool by combining data with advanced neuroimaging methods from the dMRI/functional MRI spectrum.

2. Materials and methods

The interaction between the Lead-DBS and OSS-DBS software packages adapted for DBS rat models and the input data used is visible in Fig. 1. The workflow includes the selection of suitable rat brain atlases (as described in chapter *Imaging and Atlas Data*) to define the target coordinates for DBS in the rat and the subject-specific localization of the electrodes. Estimating the VTA using OSS-DBS based on electrode localizations achieved with Lead-DBS and applied stimulation parameters is possible. In total, we examined eleven rats at two sites. The trials at the two sites took place subsequently to each other. First, in Rostock, we tested a protocol for creating postoperative CT scans. While in Rostock, we did histological examinations on one animal. In Würzburg, we examined all animals histologically. The protocols for creating postoperative CT scans and *post-mortem* electrode placement using histology differed at the two sites. However, this will render the results of our study more robust to variance in methods across groups.

2.1. Animals

We performed DBS electrode implantation procedures at the Department of Neurology in Rostock (University Medical Center Rostock, Germany) and the Department of Neurology in Würzburg (University Hospital of Würzburg, Germany). All rats were housed under temperature-controlled conditions in a 12 h light-dark cycle with water and food *ad libitum*. All animal experiments were conducted according to European guidelines (2010/63/EU) and with permission of the local animal care committee (Rostock: LALLF M-V/7221.3–1.1-051/17 and Würzburg: RUF-55.2.2–2532–2-767).

In Rostock, we examined six male adult WI (Han) rats (Charles River Laboratories, Sulzfeld, Germany) (animals r1-r6). Five male adult SD rats (Charles River Laboratories, Sulzfeld, Germany) were studied in Würzburg (animals w1-w5).

2.2. Electrodes and surgery

We employed four customized monopolar platinum electrodes with Polyimide insulation (3 μm) and one PI-SNEX-100 electrode (both types manufactured by Microprobes (Gaithersburg, USA) in Rostock. The monopolar electrodes had a rounded tip and a diameter of 225 μm. They were implanted stereotactically. We targeted the dorso-lateral subthalamic nucleus (STN) unilaterally. The target coordinates were defined relative to bregma as anterior-posterior −3.8 mm, medio-lateral

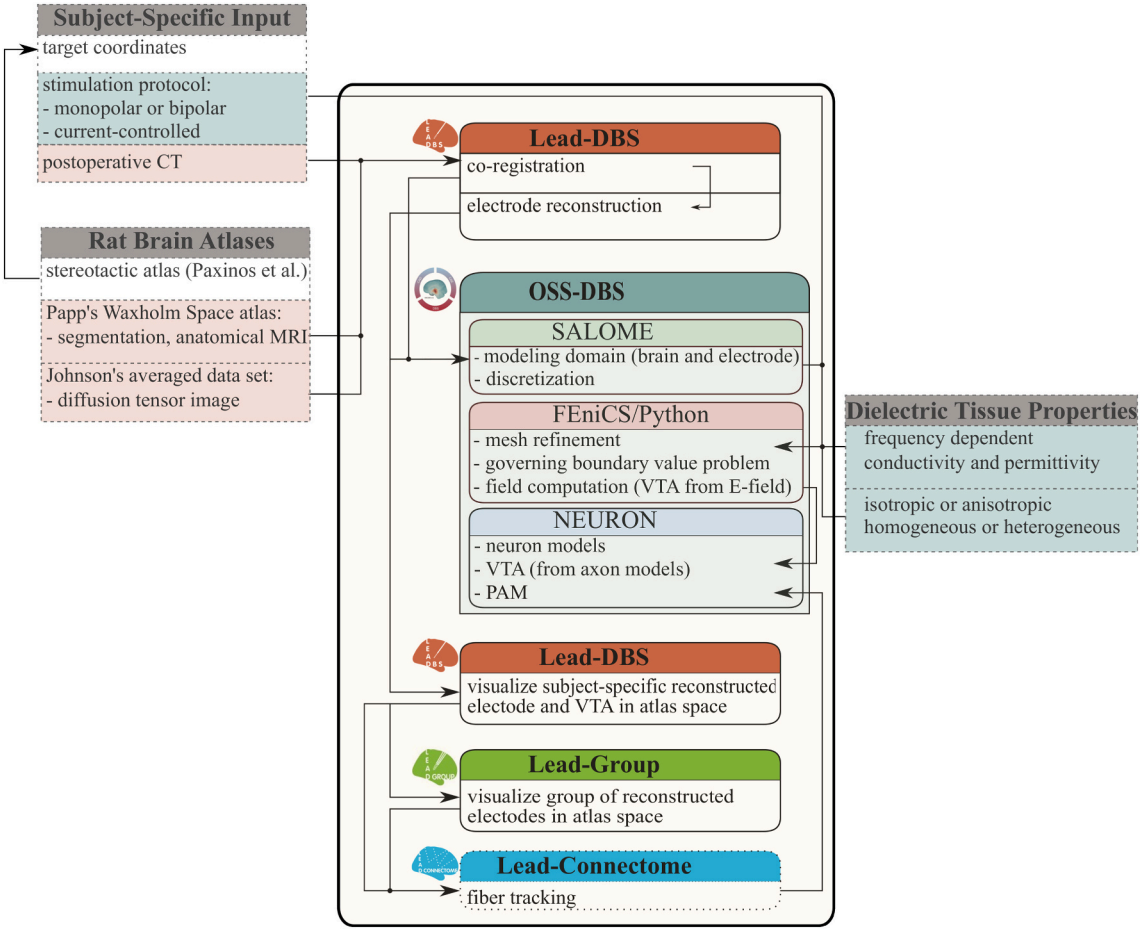

Fig. 1. Methodological Workflow: Middle: Linkage of open-source software Lead-DBS (Lead-Group/Lead-Connectome www.lead-dbs.org; Horn et al., 2019a) and OSS-DBS (https://github.com/SFB-ELAINE/OSS-DBS; Butenko et al., 2020) adapted for deep brain stimulation (DBS) in rat models. Left: Input data are the subject-specific input (including but not limited to the intended target coordinates as well as postoperative computer tomography (CT)) and the imaging data derived from rat brain atlas input (including but not limited to segmented magnetic resonance imaging (MRI) data). Right: The dielectric tissue properties are the other required input. Results are either volume of tissue activated (VTA) based on a representation of the electric field (*E*-field) or axonal models. Also, pathway activation models (PAM) along specific fiber tracts can be used. Additionally, it is possible to represent reconstructed electrode trajectories in groups in the context of the used digital brain atlases.

−2.4 mm, and dorso-ventral −7.6 mm based on the "Rat Brain Atlas" by Paxinos and Watson (2007) (P&W atlas). In one animal (r6), an infection occurred at the implantation site with an accompanying dislocation of the electrode, leading to its exclusion from further studies. Nevertheless, postoperative CT scans were performed and clearly showed the dislocation.

In Würzburg, customized monopolar Platinum/Iridium electrodes (UE-PSEGSECN1M; FHC Inc., USA) insulated with epoxy (12.5 µm) were implanted using the stereotactic P&W atlas coordinates at anterior-posterior −3.6 mm, medio-lateral −2.5 mm (right), and dorso-ventral −7.7 mm. These monopolar electrodes had a diameter of 125 µm, tapered tips, and an approximate length of 120 µm, with a diameter of less than 1 µm at the tip. Only a tiny portion of the insulation at the tip was etched away, forming the monopolar electrode contact.

The rats were not stimulated either in Rostock or Würzburg. Nevertheless, it is interesting to note that it would be possible to use the SNEX-100 electrode for both monopolar and bipolar DBS, unlike the customized monopolar electrodes.

2.3. Tissue processing and Nissl staining

Histological staining was performed as *post-mortem* electrode position control for one animal (r2) at the Department of Neurology in Rostock (University Medical Center Rostock, Germany), and for five animals (w1 – w5) at the Department of Neurology in Würzburg (University Hospital of Würzburg, Germany) to verify the correct DBS electrode placement in the vicinity of the STN.

In Würzburg, 40 µm PFA-fixed cryosections were mounted on object slides and dried for 4 h at room temperature. The sections were then incubated in cresyl violet solution (1 g cresyl violet +10 ml 100% acetic acid ad 1 l distilled water) for 30 min at room temperature. After washing in distilled water, the sections were dehydrated in ethanol and then incubated in xylene solution. Similarly, Nissl staining was conducted in Rostock, as described in detail in Supplement A. The coronal brain slices had a thickness of 30 µm (Fauser et al., 2021).

To determine electrode placement, two anatomical experts in Rostock and Würzburg (MK and CI, respectively) identified anatomical landmarks, including the STN and other landmarks close to the electrode's tip (such as the supraoptic tract (sox) and optic tract (opt)). After the identification, they matched the landmarks to the corresponding ones in analogous coronal sections of the P&W atlas. Thereby, these experts ascertained the stereotactic P&W atlas coordinates of the tip. After this landmark identification, an expert visually tracked the trajectories of the electrodes in the adjacent sections. Nonetheless, the microscopic dimensions of the electrode further complicated the identification.

2.4. Imaging and atlas data

Postoperative CT images were acquired 3–6 weeks after surgery to examine chronically implanted DBS electrodes (Table C.1). We performed this acquisition at the Core Facility Multimodale Kleintierbildgebung (Rostock University Medical Center, Germany) and the Department of Nuclear Medicine and Comprehensive Heart Failure Center (University Hospital of Würzburg, Germany) for all animals.

In Rostock, we conducted postoperative CT scans with a lethal overdosage of Ketamine/Xylazine (300 mg/kg Ketanest, 15 mg/kg Rompun) in five rats (including animal (r6) with the infection). In one animal (r2), the same was done *in vivo* under isoflurane anesthesia (5% initial dose for 1 min and 2% steady-state, 0.8 l/m oxygen flow). Detailed scanner settings for the postoperative CT scans are described in Supplement B. The postoperative CT scans were acquired on a Siemens Inveon PET/CT Multimodality System for laboratory animals (Inveon®, Siemens Healthcare Knoxville, USA) with an isotropic voxel size of 24 μm. In Würzburg, we acquired postoperative CTs *in vivo* on a U-SPECT system (U-SPECT5/CT *E*-Class; MILabs, Utrecht, The Netherlands). Data were reconstructed to an isotropic voxel size of 70 μm.

Neither preoperative nor postoperative MRI scans were acquired. Instead, postoperative CTs were directly co-registered to the T2-star weighted MRI of the Waxholm Space (WHS) atlas of the SD rat brain (Papp et al., 2014). These *ex vivo* MRIs of one adult male SD rat (postnatal-day 80, 397.6 g) have an isotropic voxel size of 39 μm. Of note, the pipeline (as adapted from human neuroimaging) would allow registration to preoperative MRI acquired in each animal individually (see below). The MRI data is later (compare chapter *OSS-DBS for DBS Field Computations*) used to define the location of the dielectric tissue properties. With that, the electric potential distribution, VTA, and PAM are computed (see also chapter *Volume of Tissue Activated and Pathway Activation Models*). It is important to note that an isotropic voxel size of the MRI data is preferable to achieve a uniformly good representation of the tissue in the *in silico* model.

2.5. Pipeline adaptation: lead-DBS for the rat

Postoperative CT scans were co-registered to the WHS atlas of the SD rat brain (Papp et al., 2014) using Lead-DBS. This co-registration was done independently by the two users (AA and NL) for each acquired postoperative CT data set. The resolution of the WHS atlas was decreased to speed up the procedure. As a result, the T2-star weighted MRI that defines the template space was resliced from 39 μm to 50 μm. We chose a resolution of 50 μm because both rat DBS electrode diameters both from Rostock and Würzburg (225 μm and 125 μm, respectively) could still be depicted. Also, the averaged dMRI data by Johnson et al. (2012), which, as described below, was used for modeling anisotropic tissue properties, has a resolution of 50 μm as well. Based on our experience, the orientation of imaging data can vary between different scanner systems. Therefore, before co-registration and localizing the electrode, postoperative CT data was reoriented to a right-anterior-superior direction.

Afterward, the postoperative CT data was roughly aligned to the WHS atlas brain and finally cropped to only the brain and skull using 3D Slicer (https://www.slicer.org; Pieper et al., 2004; Pieper et al., 2006). As stated by Borg et al. (2015), these preliminary steps improved the co-registration results. Linear co-registration (rigid and affine) of the postoperative CT data to the T2-star weighted MRI of the WHS atlas was then carried out using Advanced Normalization Tools (ANTs) (http://stnava.github.io/ANTs/; (Avants et al., 2011)) as included in Lead-DBS. Alternatively, the Lead-DBS pipeline would allow a preoperative MRI of the animal, which could subsequently be used for nonlinear registrations with the atlas, as is standard in the human pipeline (Horn et al., 2019a). However, compared to human DBS patients, the rat brain anatomy is more homogeneous across animals, as also summarized in Table C.2. It is believed that strains such as the SD rats or WI rats will be applicable for atlas-based stereotactic procedures such as DBS because of their uniform size (Paxinos and Watson, 2007). Based on this assumption, the use of postoperative CT scans and their co-registration to the WHS atlas could be seen as semi-subject-specific.

Thus, as a first approximation, it can be assumed that the localization based on this concept could be accurate enough and that preoperative scans (MRI and CT) are not mandatory. Furthermore, all animals were very similar in age, size, and weight at the time of implantation. Although from two different strains, only male adult animals were studied. After successful co-registration, which was visually approved and repeated/refined, if necessary, the electrode trajectories were reconstructed manually using Lead-DBS. For this purpose, the electrode tip and a point on the electrode trajectory were picked in the co-registered CT image. This initial localization could be manually refined using a custom-built tool of Lead-DBS that allows precise adjustments of DBS localizations.

2.6. OSS-DBS for DBS field computations

Butenko et al. (2020) introduced the Python-controlled, open-source simulation platform OSS-DBS. It uses various open-source software, such as Salome (https://www.salome-platform.org/) by Ribes and Caremoli (2007) and NEURON (https://www.neuron.yale.edu/neuron/) by Carnevale and Hines (2006) to:

- generate a volume conductor model,
- solve a finite element model problem to obtain the distribution of the extracellular potential in space and time for a given stimulation protocol and,
- quantify the subsequent neural activation (see the workflow in Fig. 1).

Within OSS-DBS (Butenko et al., 2020), the electric potential distribution in the rat brain is computed by employing the electro-quasistatic approximation of Maxwell's equation (Eq. D.1) (Bondeson et al., 2005). In Supplement D, we give more details about the applied *in silico* modeling procedure. The stimulation coordinates from Lead-DBS defined the position of the electrode's tip. The Lead-DBS reconstruction also provided the trajectory of an electrode. Next, we determined the animal with the best match of the localization methods (Lead-DBS and histology, respectively) and computed the potential distribution resulting from a current-controlled stimulation. Here, we used a rectangular pulse with a width of 60 μs, a repetition frequency of 130 Hz, and a current amplitude of 200 μA (Badstübner et al., 2017; Fauser et al., 2021).

First, we approximated the VTA based on the electric field distribution. Second, we used a PAM to evaluate the activation of axon cable models placed along anatomically plausible pathways. Fibers were taken from the WHS atlas repository (https://www.nitrc.org/projects/whs-sd-atlas, S56280_fiberspline.trk) and derived from dMRI data. The simulation considered only fibers that passed the STN within a radius of 2 mm and were at least 3 mm long.

3. Results

3.1. Histological electrode localization

For animal r2, the comparison of the histological sections with the stereotactic atlas and the visual determination of the distance between the puncture channel and the STN resulted in an approximate position of the electrode of anterior-posterior −3.84 mm, medio-lateral −1.59 mm, and dorso-ventral −8.31 mm in the stereotactic P&W atlas coordinates. Consequently, the offset of the localized coordinate to the intended stimulation target was anterior-posterior 0.105 mm, medio-lateral 0.810 mm, and dorso-ventral −0.385 mm. Negative offsets represent a localized coordinate further posterior, lateral, or ventral than planned.

The tip locations in all five SD rats from the Würzburg site were estimated similarly. The mean value and the standard deviation, as presented in Table F.1, of the approximate tip position in the five rats were anterior-posterior −3.24 ± 0.29 mm, medio-lateral −2.86 ± 0.20 mm, and dorso-ventral −8.08 ± 0.38 mm in the stereotactic P&W atlas coordinates. This procedure resulted in an offset to the intended stimulation target of anterior-posterior 0.47 ± 0.24 mm, medio-lateral −0.36 ± 0.20 mm, and dorso-ventral −0.06 ± 0.38 mm (as summarized in Table F.2). All electrodes were found to be placed in a more lateral and anterior position. Three of the five electrodes were located more in ventral than dorsal direction relative to the corrected stereotactic coordinates. The latter are the planned stereotactic coordinates updated by a linear registration based on the animals' weight, as described in Supplement E.

3.2. Electrode localization via postoperative CT

Beam hardening effects from the metallic electrode and the metallic fixation screws to the skullcap occurred in all postoperative images (Fig. 2 &Fig. 3). In animal r2, we observed an artifact in the postoperative CT image showing two electrodes, likely due to breathing. The absence of the second electrode in scans performed with a different scanner setting for the same animal, given in Supplement B, confirmed that it was indeed an artifact. The scanner setting (set2) used for this animal (r2) showed similarly promising results as the scanner setting (set1) used for the other animals.

We checked and manually approved all co-registrations between postoperative CTs and atlas in all animals. To do so, in Lead-DBS, an overlay view of red wires representing an edge-detected version of the T2-star weighted MRI, including soft tissue structures and skull, as shown in Fig. 3, was used. In the overlays, the users (AA and NL) compared distinct structures of the skull. Deviations (of approximately 100 μm) between the osseous structures of the T2-star weighted MRI and the postoperative CT were deemed acceptable if they did not occur in the vicinity of the target region.

The results of the localized coordinates are summarized in Table F.1. For the group of animals from Rostock, the means and the standard deviations in WHS coordinates were anterior-posterior −3.18 ± 0.48 mm, medio-lateral 2.61 ± 0.77 mm, and dorso-ventral −0.83 ± 0.10 mm. For the group of animals from Würzburg, the WHS coordinates were anterior-posterior −2.71 ± 0.46 mm, medio-lateral 2.69 ± 0.23 mm, and dorso-ventral −0.64 ± 0.15 mm.

3.3. Comparison of histological and lead-DBS localizations

A visual comparison between localizations based on histology and Lead-DBS is shown in Fig. 4 and Supplement G (Fig. G.1 to Fig. G.5). We compared the position of the determined positions of the electrodes to landmarks that are recognizable in all images respective to the corresponding atlases. As landmarks, the optic tract (opt), internal capsule (ic), dorsal part of the third ventricle (D3V), as well as the lateral ventricle (LV), field CA1 – CA3 of the hippocampus, and the corpus callosum (cc) were evident in all images. In cases in which the STN was clearly identified, it was also used to characterize the localized tip of the electrode. In animal w2, the electrode tip was located in the STN at its dorsal border based on both reconstruction techniques, as shown in Fig. 4. Here, the coordinates of the electrode tip determined with Lead-DBS in the postoperative CT scans using the WHS atlas suggested a more dorsal position than the histological localization method. The electrode-position determination by both ways showed that the electrode tip in animal w4 was not located close to the STN but considerably more anteriorly in the EP.

Using different atlas systems with comparable but different coordinate systems (WHS *vs.* P&W), it was not immediately possible to determine the offset between the coordinates localized with Lead-DBS and the histological coordinates and the intended target coordinates. We selected the distances relative to bregma and anterior commissure in the postoperative CTs co-registered to the WHS atlas, as described in Supplement E and shown in Fig. E.1, to estimate the offset between both localization methods. By defining the distances relative to bregma and ac, we demonstrated that the RMSE between the localizations based on histology and Lead-DBS did not exceed 1 mm in animals w1–5, as summarized in Table F.2. While for the offsets relative to bregma, the anterior-posterior direction showed the highest RMSE with 0.64 mm, the dorso-ventral direction of the offset relative to anterior commissure featured its largest RMSE with 0.70 mm. In the medio-lateral direction, the offsets relative to bregma and anterior commissure were similar (RSME of 0.27 mm and 0.31 mm, respectively). As visualized in Figs. F.1 and F.2, the results showed high inter-rater agreement between the two users of Lead-DBS (AA and NL).

3.4. Group visualization and 3D trajectories

When using histology, the electrode tip can be localized relative to the intended target structures. However, the creation of an overview of localized electrodes on a group level is challenging. A vital advantage of the Lead-DBS method and its sister application, Lead-Group (Treu et al., 2020), is the possible visualization of a group of reconstructed electrodes concerning the target and surrounding structures, as shown in Fig. 5. With this method, a possible tilt of the implanted electrode can also be made visible.

3.5. Volume of tissue activated and pathway activation models

For animal w2, for which the best match to the intended stimulation coordinates was estimated, we calculated bioelectrical effects to demonstrate the interface's capability between Lead-DBS and OSS-DBS as well as the advanced computational methods OSS-DBS. An estimate of the VTA, as defined by thresholding the vector magnitudes of the electric field (Fig. 6 B)), was computed. Visualizing the reconstructed electrodes and their simulated VTAs made it possible to estimate the influence of the stimulation on the surrounding tissue. The VTA was pictured with distinct target structures (STN and entopeduncular nucleus (EPN)) and well-defined structures in the P&W atlas (ac, mt, and sox) (Fig. 6 A)). In addition, Lead-DBS, combined with its sister application Lead-Connectome, and OSS-DBS offer the possibility to display

Fig. 2. An exemplary postoperative CT scan: of one rat's (animal r1; left) entire head, which also shows the fixation of the DBS electrode to the skull. The latter comprised adhesive mounting and three screws (Lense head screws, similar to DIN 7981, stainless steel A2, 1 × 3 mm, Minischrauben.com, Hofkirchen, Germany). The adhesive mounting consisted of a bonding agent (Heliobond, Ellwangen, Germany) and dental cement (Luxatemp Automix Plus, A2, DMG Chemisch-Pharmazeutische Fabrik GmbH, Hamburg, Germany). The skull (right) close-up shows beam hardening effects due to the metallic DBS electrode and fixation screws, which appeared as typical interference ripples anterior to the electrode.

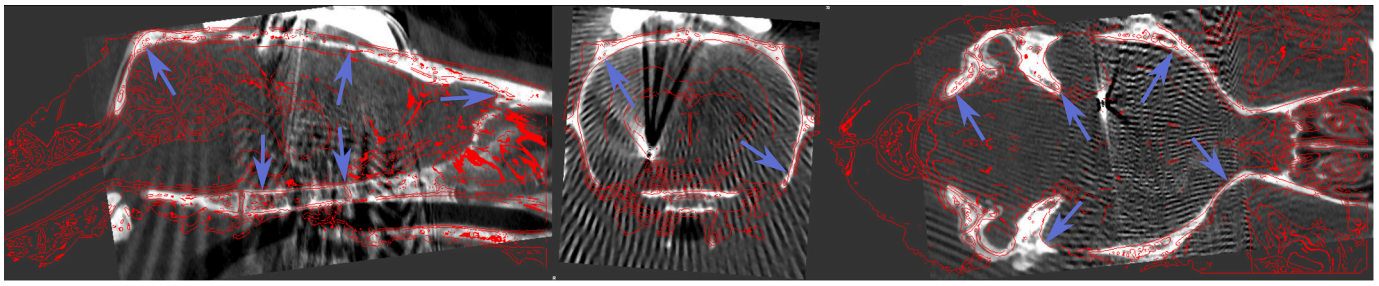

Fig. 3. Co-registered postoperative CT: shown as a gray-scale image of the animal (r1) and overlaid over the T2-star weighted MRI of the WHS atlas (Papp et al., 2014). The red wires represent the outlines of the T2-star weighted MRI of both the soft tissue and the skull. Distinct structures of the skull were used to ensure a good co-registration as marked by arrows. Challenges in evaluating usual landmarks (bregma and lambda) are due to their covering by dental cement and beam hardening effects caused by the metallic electrode. The offset between the osseous structures visible here is approximately 50 μm. Thus, the co-registration can be regarded as successful. (For interpretation of the references to color in this figure legend, the reader is referred to the web version of this article.)

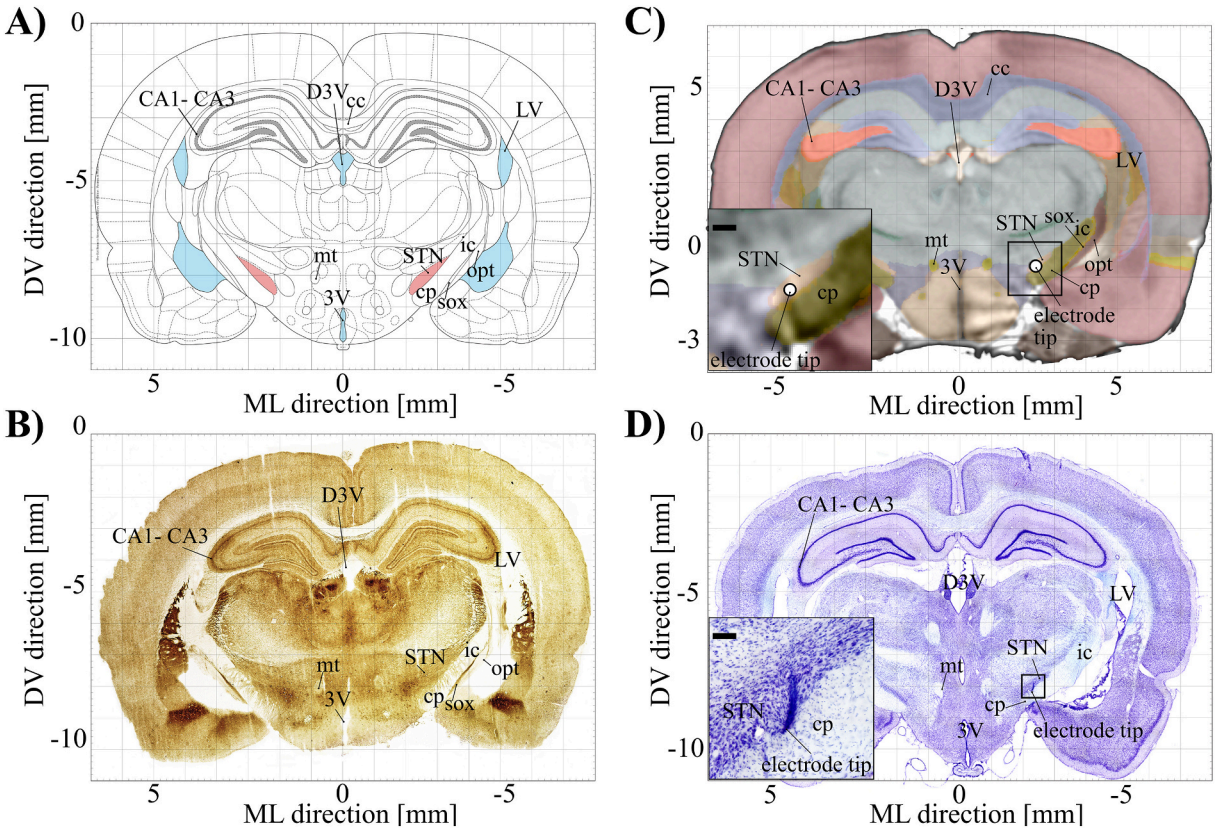

Fig. 4. Visual Comparison Animal w2: Schematic drawing (A) and histological plate (B) adapted from the P&W atlas at anterior-posterior −3.60 mm relative to bregma. The coronal plate, including the electrode tip, is shown for Lead-DBS in the WHS atlas space (C) and a Nissl section (D). Images (A) and (B) were adapted from the P&W atlas (Paxinos and Watson, 2007) with the publisher's permission. Image (C) is an overlay of the T2-star weighted MRI (gray-scale image) and the WHS atlas in transparent colors (Papp et al., 2014). Abbreviations of the anatomical landmarks are defined as subthalamic nucleus (STN), lateral ventricle (LV), (dorsal) 3rd ventricle ((D)3 V), field CA1-CA3 of the hippocampus (CA1-CA3), corpus callosum (cc), cerebral peduncle (cp), internal capsule (ic), mammillothalamic tract (mt), optic tract (opt), supraoptic tract (sox), and scale bar of inset in (C) 200 μm as well as (D) 100 μm. To improve the comparability of the images, we manually adjusted the sections' size to the P&W atlas.

fibers and evaluate their recruitment by the DBS signal as shown in Fig. 6 D (red - 'recruited,' purple - damaged or non-physiological). This assessment of stimulation extent is achieved by:

- allocating passive models of myelinated axons along the fibers,
- computing the electric potential distribution on the axonal compartments, and
- solving the Frankenhaeuser-Huxley-based equation to probe the excitability of the axon models by the extracellular stimulus.

4. Discussion

It was demonstrated in human DBS research that electrode displacements of a mere ~2 mm might lead to drastic changes in effectivity in established DBS cases such as Parkinson's Disease (Horn et al., 2019a). In rodents, DBS electrodes are mainly localized using *post-mortem* histology. The disadvantage of this method is that it cannot be performed on live animals. Thus experimental choices are limited. Also, potentially, larger animal cohorts become necessary. Other groups have used neuroimaging methods to localize DBS electrodes in the past. For

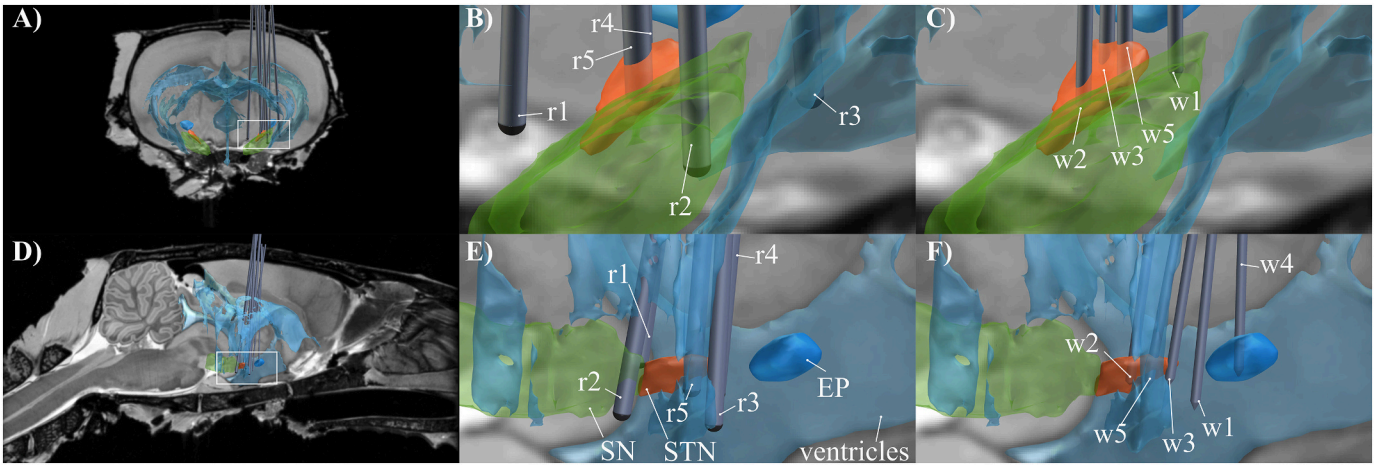

Fig. 5. Group visualization of the electrodes reconstructed in all animals in coronal (A) and sagittal view (D). The coronal view shows the magnification of the groups r1-r5 (B) and w1-w5 (C). The sagittal view shows the magnification of the groups r1-r5 (E) and w1-w5 (F). Also depicted are the ventricular system, subthalamic nucleus (STN), entopeduncular nucleus (EP), and substantia nigra (SN) in coronal (top row) and sagittal view (bottom row).

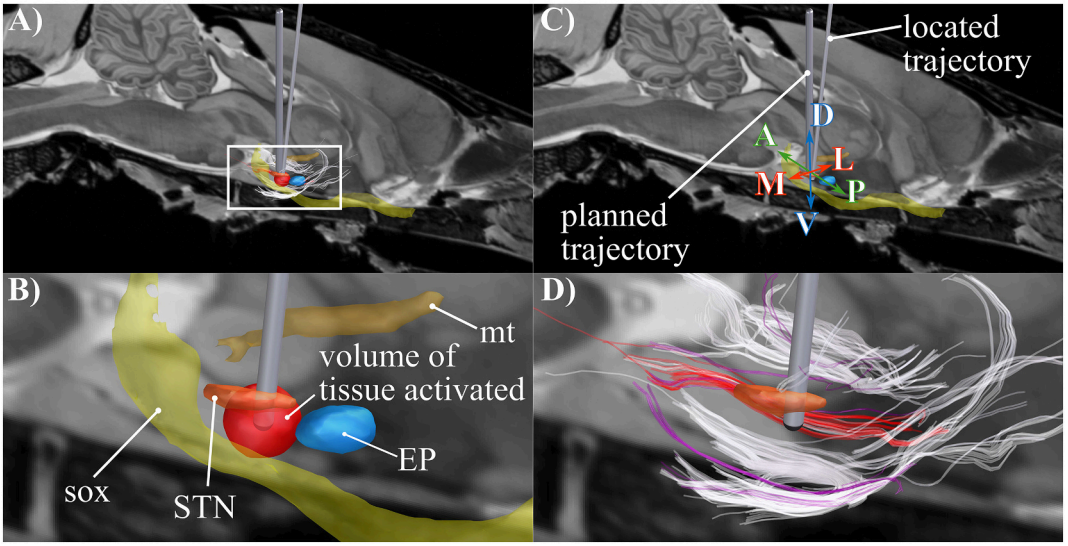

Fig. 6. Potential Applications: A) is an overview: B) shows the volume of tissue activated (VTA) (based on electric field thresholding and computed with OSS-DBS) in animal w2, caused by a monopolar electrode design with a rectangular pulse (with a pulse width of 60 μs, a current amplitude of 200 μA, and a pulse repetition frequency of 130 Hz) with distinct brain structures (subthalamic nucleus (STN), entopeduncular nucleus (EP), anterior commissure (ac = Waxholm space origin), supraoptic tract (sox), and mammillothalamic tract (mt)). C) shows a planned trajectory of a DBS electrode in the target region, which can be varied in dorsal (D), ventral (V), anterior (A), posterior (P), lateral (L), and medial (M) direction. In addition, D) shows the pathway activation based on fiber tracts derived from diffusion tensors obtained from diffusion-weighted MRI imaging data of the WHS atlas (Papp et al., 2014). Activated fibers are red, not-activated fibers white, damaged fibers magenta. Fibers were taken from the WHS atlas repository (https://www.nitrc.org/projects/whs-sd-atlas, S56280_fiberspline.trk). (For interpretation of the references to color in this figure legend, the reader is referred to the web version of this article.)

instance, Zhao et al. (2020) applied graphene electrodes (which led to fewer MRI artifacts). They scanned rats to investigate the relationship between DBS and functional MRI pattern activations (Zhao et al., 2020). Similar to our approach, Rangarajan et al. (2016) and Király et al. (2020) used MRI and CT to localize DBS electrodes *in vivo* in rats and mice, respectively. A few similar methodological papers exist. To the best of our knowledge, we provide the first open-source toolbox. It is standardized to localize DBS electrodes in rodents and subsequently simulate the stimulation effect on neuronal tissue.

The skull landmarks (bregma and lambda) would have been the first choice to evaluate the accuracy of the co-registration of CT and MRI. However, in the postoperative CT scans, these landmarks are obscured by the adhesive mounting and the screws used to fixate the electrodes. The use of preoperative scans could circumvent this problem. When using preoperative CT scans as the basis for the manual co-registration of postoperative CT scans, as described by Király et al. (2020), the time gap between the preoperative and postoperative measurements has to be considered when the animals continue to grow. If the position of the electrode in the chronic state is to be characterized (2–3 weeks after surgery), the animal has already developed further, and a manual co-registration of the images based on osseous landmarks (as done by Király et al. (2020)) is no longer feasible. Though not performed in the current study, co-registering subject-specific MRIs is already implemented in Lead-DBS, which is on hand for rat DBS models in future studies.

4.1. Comparison between histological and lead-DBS localizations

In the present feasibility study, our main aim was to establish an adjustable open-source pipeline to localize DBS electrodes in rats (or

other rodents of similar size). Our results showed a high inter-rater agreement. Using Lead-DBS, the electrode tip was localized further dorsal than histologically defined. This finding resulted from the visual comparison of both localization methods and the consideration of the offset relative to the bregma and anterior commissure.

Several factors could have played a role here: The MRI-based method could have been flawed due to image resolution or co-registration inaccuracies. Yet, high inter-rater reliability speaks against the latter reason. Second, the two methods use different coordinate systems (bregma and WHS origin in the anterior commissure). Third, different strains were used to define the atlas space: brain slices of a WI rat for the stereotactic P&W atlas, and the WHS atlas an SD rat was imaged. Finally, histological localization of the electrode tip and trajectory could be less accurate than assumed. Damage to the brain tissue caused, *e.g.*, by the extraction of the electrode, might have resulted in the tearing of the tissue under the electrode, which may explain the dorso-ventral discrepancy.

Further comparative studies are needed to define more precisely which method is superior for which scientific question. The assessment of the correct placement within a specifically stained target region may only be possible using histology. However, the imaging method could (potentially) bring a sort of "model-based" three-dimensional view to the matter that could make electrode localizations more comparable across animals, cohorts, and even research centers (as shown in Fig. 5). A similar development was observed in the human DBS field (Horn, 2019; Treu et al., 2020).

4.2. Limitations

Several limitations apply to the present study, some of which we already touched upon in the section above. Assuming that the rat brain is ~0.15% in size compared to a human brain (~2 g *vs.* ~1350 g is usually reported in textbooks), the applied 50 μm isotropic imaging resolution was superior to that one in human DBS studies (classically ~0.5–1 mm). Nevertheless, distortion artifacts and misregistrations cannot be ruled out, and further confirmation studies (especially using electrode phantoms) should be carried out. In some cases, we encountered better co-registration results when registering the postoperative CT images to the WHS atlas T2-star weighted MRI with a resolution of 39 μm before co-registering them to the resliced WHS atlas T2-star weighted MRI with a 50 μm resolution. For this reason, we recommend using the best possible resolution, especially for co-registration, if the appropriate computational hardware and time are available. The most critical limitation is that we directly co-registered postoperative CTs to an MRI atlas of the rat instead of to high-resolution MRIs of the same animal. Our experience from human DBS imaging would favor the latter approach, which should optimally be investigated in upcoming studies (in present animals, no preoperative imaging could be acquired). However, any *in vivo* imaging procedure, such as MRI, dMRI, or CT, is conducted under general anesthesia. This procedure is associated with a particular animal strain, *e.g.*, during induction and termination of anesthesia. Therefore, it is crucial to do only as many *in vivo* imaging procedures as necessary.

It can be generally assumed that inter-animal anatomy is not as different in the field of rodent DBS as it is in humans, in whom significant variations in gyrification occur. The cortical folds of rodents, on the other hand, are minimal and well comparable across animals. Nonetheless, differences between animal strains (WI and SD) have been described before. The midbrain and hindbrain of WI rats are longer in the anterior-posterior direction than those of SD rats (Khan et al., 2018). In addition, renownedly a transformation between different rat brain atlases, *e.g.*, the P&W atlas (Paxinos and Watson, 2007) and the Swanson atlas (Swanson, 1998) based on different strains (WI and SD) and animal weights is not straightforward.

Another unknown factor to consider is the reliability of the registration of sections between different atlases. The same holds for the transformation between coordinates derived from digital atlases, which differ in resolution, animal strains, weights, and *ex vivo* or *in vivo* imaging (Barrière et al., 2019; Johnson et al., 2012; Papp et al., 2014). When high-resolution preoperative data are available, some advanced methods already established in Lead-DBS could be applied.

Moreover, *ex vivo* MRI and CT scans in animals exhibit a much better resolution than *in vivo* scans. This lower *in vivo* resolution is mainly caused by technical limitations (scan time and radiation dosage) and possible breathing artifacts. The same holds for dMRI. On the other hand, *ex vivo* imaging has limitations as well. These include, among others, the underestimation of the ventricle size, as the cerebrospinal fluid drains from the ventricles *post-mortem*. This fluid drain leads to a collapse of the ventricles. As described by Llambrich et al. (2020), specialized CT techniques manage to avoid this difficulty and create CT images that depict the skull and detailed brain tissue. However, the necessity to fixate the brains in, *e.g.*, resin makes subsequent histological examinations impossible (Masís et al., 2018).

The fact that histology has been used and is established (*i.e.*, should be considered the status quo or gold standard) does not automatically mean that the method is accurate. In more detail: while we believe that histological determination of the electrode placement relative to the target structures is correct, the *exact coordinates* determined by histology could be imprecise for the reasons mentioned above (*e.g.*, tissue shearing, sectioning, deformation of the brain after extraction, *etc.*). We qualitatively compared single case examples (*e.g.*, within / outside of the STN). These examples showed good agreement between the methods and indicate that, indeed, both sources are correct. The localization of the electrode of animals w2 and w4 can be cited here as examples. While in animal w2, the STN was hit in the middle, in animal w4 the EP was hit unintentionally. Both were evident by Lead-DBS as well as in the histological sections. Such a displacement along the anterior-posterior axis, as shown here or less pronounced, can lead to direct activation of the EP or substantia nigra (Butenko et al., 2019).

4.3. Outlook

An advantage of our tool is that the code already established in humans could be reused. This fact would also allow the incorporation of putative clinical, methodological novelties for the rodent pipeline (and *vice versa*). Since the initial publication of Lead-DBS in 2014 (Horn and Kühn, 2015), a more extensive series of methodological advances have shaped a learning curve of ever more precise localization approaches – all of which are automatically included in the present tool for rats. Though no animal-specific preoperative scans were used in the present study, the pipeline is perfectly capable of having them.

As we advance, optimal protocols would generate high-resolution multispectral MRIs from animals after DBS implantation and before surgery and postoperative CT. Lead-DBS works seamlessly with its sister-application Lead-Connectome (Horn et al., 2014; Horn and Blankenburg, 2016), which can also be used for rodent data. Hence, preoperative or postoperative dMRI or resting-state functional MRI data may be processed and directly incorporated with Lead-DBS results. Beyond connectivity estimation, the former can also support a more precise definition of tissue activation using OSS-DBS (Butenko et al., 2020) and its PAMs.

So far, Lead-DBS includes and OSS-DBS supports both electrode designs presented in this study (SNEX-100; *i.e.*, bipolar stimulation; as well as the monopolar configuration from Rostock). The electrode design in rodent studies is essential. Butenko et al. (2021) ascertained that field focalization in the STN for dorsal implantations depends on the design. As the tool may become more widespread, adding additional geometries to the pipeline would be uncomplicated. Designs exclusively built for recording rather than stimulation as described by (Borg et al., 2015; Kastner et al., 2020; Masís et al., 2018) could be supported, as well.

OSS-DBS also offers to investigate realistically set axonal populations. The recruitment of fibers during DBS is of interest in the context of pathway activation studies and can be simulated with the

combined use of Lead-DBS and OSS-DBS. Clinical Parkinson's disease research demonstrated that stimulation of specific pathways, such as the cortico-subthalamic projections, correlates with alleviating symptoms in patients. At the same time, the recruitment of other pathways can cause detrimental effects, *e.g.*, stimulation of internal capsule fibers of passage invokes motor contractions. Therefore, the evaluation of the pathway activation is a highly relevant tool to understand the DBS mechanism better and provide a better translatability of the animal research findings. Incorporating the atlas and co-registration algorithms for rats in Lead-DBS gives users access to automated routines for modeling the pathway activation implemented in OSS-DBS.

Further methodological advances include the capability of manual refinements of normalization warp fields using manually placed point-fiducials (Edlow et al., 2019), already implemented within Lead-DBS. This method could be directly used to improve electrode placement accuracy, especially in cases where detailed preoperative data are available. Since Lead-DBS allows the visualization of the stereotactic plan of the electrode trajectory (as shown in Fig. 6 C)), potential stimulation targets may be evaluated in advance, *i.e.*, before surgery. Even if not performed preoperatively for all animals, this could be applied in individual cases to augment the study design. In combination with OSS-DBS, this approach could also be used to obtain an *in silico* assessment of the effects of stimulation protocols. These effects may result from the specific geometry of the electrode contacts, the stimulation amplitude, the stimulation frequency, the pulse duration of DBS, or a combination thereof.

5. Conclusions

This study presents an adaptation of a well-established simulation pipeline widely used in human DBS research (Lead-DBS) for application in rat-model DBS. We incorporated an interface to a biophysical modeling toolbox (OSS-DBS) that can be used to precisely model the modulatory impact of DBS onto the biological tissue. We make this novel joint pipeline openly available. The reproducibility of DBS electrode localizations by two independent users is one demonstration of its capability. Our comparison of results from MRI-based (*i.e.*, Lead-DBS) electrode localizations *versus* conventional histology-based localizations also underlines the great potential of this simulation pipeline. We envision potential novel applications that could include combinations of advanced neuroimaging methods with models of DBS in rodents.

Funding

Rostock (AA, KB, MK, MF, AS, and UvR): This work was funded by the Deutsche Forschungsgemeinschaft (DFG, German Research Foundation) – SFB 1270/1–299150580 as well as in the scope of the Research Training Group GRK 1505 welisa and the Department of Life, Light and Matter, University of Rostock.

Berlin (AH, NL, AK): This work was funded by the DFG Project-ID 424778381-TRR 295. AH was in addition supported by the DFG, Emmy Noether Stipend 410169619, as well as by the Deutsches Zentrum für Luft- und Raumfahrt (DynaSti grant within the EU Joint Programme Neurodegenerative Disease Research, JPND) as well as the Foundation for OCD Research (FFOR). AH is a participant in the BIH-Charité Clinician Scientist Program funded by the Charité –Universitätsmedizin Berlin and the Berlin Institute of Health.

Würzburg (CI, JZC, TH): CI was funded by the DFG Project-ID 424778381-TRR 295. JC was funded by the China Scholarship Council. The imaging study at the University Hospital of Würzburg was supported by funding of the Federal Ministry of Education and Research for the Comprehensive Heart Failure Center (BMBF; 01EO1504).

All authors have read and agreed to the published version of the manuscript.

Declaration of Competing Interest

None.

Appendix A. Supplementary data

Supplementary data to this article can be found online at https://doi.org/10.1016/j.expneurol.2022.113978.

References

Akram, H., Sotiropoulos, S.N., Jbabdi, S., Georgiev, D., Mahlknecht, P., Hyam, J., Foltynie, T., Limousin, P., De Vita, E., Jahanshahi, M., Hariz, M., Ashburner, J., Behrens, T., Zrinzo, L., 2017. Subthalamic deep brain stimulation sweet spots and hyperdirect cortical connectivity in Parkinson's disease. NeuroImage 158, 332–345. https://doi.org/10.1016/j.neuroimage.2017.07.012.

Al-Fatly, B., Ewert, S., Kübler, D., Kroneberg, D., Horn, A., Kühn, A.A., 2019. Connectivity profile of thalamic deep brain stimulation to effectively treat essential tremor. Brain J. Neurol. 18, 130. https://doi.org/10.1093/brain/awz236.

Alho, E.J.L., Di Lorenzo Alho, A.T., Grinberg, L., Amaro, E., Santos, G.A.B., Silva, R.E., Neves, R.C., Alegro, M., Coelho, D.B., Teixeira, M.J., Fonoff, E.T., Heinsen, H., 2017. High thickness histological sections as alternative to study the three-dimensional microscopic human sub-cortical neuroanatomy Eduardo Joaquim Lopes Alho, Ana Tereza Di Lorenzo Alho, Lea Grinberg, Edson Amaro, Gláucia Aparecida Bento dos Santos, et al. Brain Struct. Funct. 1–14. doi:https://doi.org/10.1007/s00429-017-1548-2.

Amunts, K., Lepage, C., Borgeat, L., Mohlberg, H., Dickscheid, T., Rousseau, M.-É., Bludau, S., Bazin, P.-L., Lewis, L.B., Oros-Peusquens, A.-M., Shah, N.J., Lippert, T., Zilles, K., Evans, A.C., 2013. BigBrain: an ultrahigh-resolution 3D human brain model. Sci. N. Y. NY 340, 1472–1475. https://doi.org/10.1126/science.1235381.

Apetz, N., Kordys, E., Simon, M., Mang, B., Aswendt, M., Wiedermann, D., Neumaier, B., Drzezga, A., Timmermann, L., Endepols, H., 2019. Effects of subthalamic deep brain stimulation on striatal metabolic connectivity in a rat hemiparkinsonian model. Dis. Model. Mech. https://doi.org/10.1242/dmm.039065 dmm.039065.

Åström, M., Lemaire, J.-J., Wårdell, K., 2012. Influence of heterogeneous and anisotropic tissue conductivity on electric field distribution in deep brain stimulation. Med. Biol. Eng. Comput. 50, 23–32. https://doi.org/10.1007/s11517-011-0842-z.

Avants, B.B., Tustison, N.J., Song, G., Cook, P.A., Klein, A., Gee, J.C., 2011. A reproducible evaluation of ANTs similarity metric performance in brain image registration. NeuroImage 54, 2033–2044. https://doi.org/10.1016/j.neuroimage.2010.09.025.

Badstübner, K., Gimsa, U., Weber, I., Tuchscherer, A., Gimsa, J., 2017. Deep brain stimulation of hemiparkinsonian rats with unipolar and bipolar electrodes for up to 6 weeks: behavioral testing of freely moving animals. Park. Dis. 2017, 1–18. https://doi.org/10.1155/2017/5693589.

Barrière, D.A., Magalhães, R., Novais, A., Marques, P., Selingue, E., Geffroy, F., Marques, F., Cerqueira, J., Sousa, J.C., Boumezbeur, F., Bottlaender, M., Jay, T.M., Cachia, A., Sousa, N., Mériaux, S., 2019. The SIGMA rat brain templates and atlases for multimodal MRI data analysis and visualization. Nat. Commun. 10, 5699. https://doi.org/10.1038/s41467-019-13575-7.

Bergman, H., 2021. The Hidden Life of the Basal Ganglia, At the Base of Brain and Mind. MIT Press.

Böhme, A., van Rienen, U., 2016. A comparative study of approaches to compute the field distribution of deep brain stimulation in the Hemiparkinson rat model. In: 2016 38th Annual International Conference of the IEEE Engineering in Medicine and Biology Society (EMBC). Presented at the 2016 38th Annual International Conference of the IEEE Engineering in Medicine and Biology Society (EMBC). IEEE, Orlando, FL, USA, pp. 5821–5824. https://doi.org/10.1109/EMBC.2016.7592051.

Bondeson, A., Rylander, T., Ingelström, P., 2005. Computational Electromagnetics, Texts in Applied Mathematics. Springer, New York, N.Y.

Borg, J.S., Vu, M.-A., Badea, C., Badea, A., Johnson, G.A., Dzirasa, K., 2015. Localization of Metal Electrodes in the Intact Rat Brain Using Registration of 3D Microcomputed Tomography Images to a Magnetic Resonance Histology Atlas. eneuro 2, ENEURO.0017-15.2015. https://doi.org/10.1523/ENEURO.0017-15.2015.

Bot, M., Schuurman, P.R., Odekerken, V.J.J., Verhagen, R., Contarino, F.M., de Bie, R.M. A., van den Munckhof, P., 2018. Deep brain stimulation for Parkinson's disease: defining the optimal location within the subthalamic nucleus. J. Neurol. Neurosurg. Psychiatry. https://doi.org/10.1136/jnnp-2017-316907 jnnp-2017-316907-7.

Butenko, K., Bahls, C., Rienen, U., 2019. Evaluation of epistemic uncertainties for bipolar deep brain stimulation in rodent models. In: 2019 41st Annual International Conference of the IEEE Engineering in Medicine and Biology Society (EMBC). Presented at the 2019 41st Annual International Conference of the IEEE Engineering in Medicine & Biology Society (EMBC). IEEE, Berlin, Germany, pp. 2136–2140. https://doi.org/10.1109/EMBC.2019.8857910.

Butenko, K., Bahls, C., Schröder, M., Köhling, R., van Rienen, U., 2020. OSS-DBS: open-source simulation platform for deep brain stimulation with a comprehensive automated modeling. PLoS Comput. Biol. 16, e1008023 https://doi.org/10.1371/journal.pcbi.1008023.

Butson, C.R., McIntyre, C.C., 2005. Tissue and electrode capacitance reduce neural activation volumes during deep brain stimulation. Clin. Neurophysiol. 116, 2490–2500. https://doi.org/10.1016/j.clinph.2005.06.023.

Caire, F., Ranoux, D., Guehl, D., Burbaud, P., Cuny, E., 2013. A systematic review of studies on anatomical position of electrode contacts used for chronic subthalamic stimulation in Parkinson's disease. Acta Neurochir. (Wien) 155. https://doi.org/10.1007/s00701-013-1782-1, 1647-54-discussion 1654.

Carnevale, T., Hines, M., 2006. The NEURON Book. Cambridge Univ. Press, Cambridge [u.a].

Casero, R., Siedlecka, U., Jones, E.S., Gruscheski, L., Gibb, M., Schneider, J.E., Kohl, P., Grau, V., 2017. Transformation diffusion reconstruction of three-dimensional histology volumes from two-dimensional image stacks. Med. Image Anal. 38, 184–204. https://doi.org/10.1016/j.media.2017.03.004.

Deuschl, G., Schade-Brittinger, C., Krack, P., Volkmann, J., Schäfer, H., Bötzel, K., Daniels, C., Deutschländer, A., Dillmann, U., Eisner, W., Gruber, D., Hamel, W., Herzog, J., Hilker, R., Klebe, S., Kloss, M., Koy, J., Krause, M., Kupsch, A., Lorenz, D., Lorenzl, S., Mehdorn, H.M., Moringlane, J.R., Oertel, W., Pinsker, M.O., Reichmann, H., Reuss, A., Schneider, G.-H., Schnitzler, A., Steude, U., Sturm, V., Timmermann, L., Tronnier, V., Trottenberg, T., Wojtecki, L., Wolf, E., Poewe, W., Voges, J., German Parkinson Study Group, N.S, 2006. A randomized trial of deep-brain stimulation for Parkinson's disease. N. Engl. J. Med. 355, 896–908. https://doi.org/10.1056/NEJMoa060281.

D'Haese, P.-F., Pallavaram, S., Li, R., Remple, M.S., Kao, C., Neimat, J.S., Konrad, P.E., Dawant, B.M., 2012. CranialVault and its CRAVE tools: a clinical computer assistance system for deep brain stimulation (DBS) therapy. Med. Image Anal. 16, 744–753. https://doi.org/10.1016/j.media.2010.07.009.

Edlow, B.L., Mareyam, A., Horn, A., Polimeni, J.R., Witzel, T., Tisdall, M.D., Augustinack, J.C., Stockmann, J.P., Diamond, B.R., Stevens, A., Tirrell, L.S., Folkerth, R.D., Wald, L.L., Fischl, B., van der Kouwe, A., 2019. 7 tesla MRI of the ex vivo human brain at 100 micron resolution. Sci. Data 6, 244. https://doi.org/10.1038/s41597-019-0254-8.

Fauser, M., Ricken, M., Markert, F., Weis, N., Schmitt, O., Gimsa, J., Winter, C., Badstübner-Meeske, K., Storch, A., 2021. Subthalamic nucleus deep brain stimulation induces sustained neurorestoration in the mesolimbic dopaminergic system in a Parkinson's disease model. Neurobiol. Dis. 156, 105404 https://doi.org/10.1016/j.nbd.2021.105404.

Grant, P.F., Lowery, M.M., 2010. Effect of dispersive conductivity and permittivity in volume conductor models of deep brain stimulation. IEEE Trans. Biomed. Eng. 57, 2386–2393. https://doi.org/10.1109/TBME.2010.2055054.

Gunalan, K., Chaturvedi, A., Howell, B., Duchin, Y., Lempka, S.F., Patriat, R., Sapiro, G., Harel, N., McIntyre, C.C., 2017. Creating and parameterizing patient-specific deep brain stimulation pathway-activation models using the hyperdirect pathway as an example. PLoS One 12, e0176132. https://doi.org/10.1371/journal.pone.0176132.

Hardman, C.D., Henderson, J.M., Finkelstein, D.I., Horne, M.K., Paxinos, G., Halliday, G. M., 2002. Comparison of the basal ganglia in rats, marmosets, macaques, baboons, and humans: volume and neuronal number for the output, internal relay, and striatal modulating nuclei. J. Comp. Neurol. 445, 238–255. https://doi.org/10.1002/cne.10165.

Horn, A., 2019. The impact of modern-day neuroimaging on the field of deep brain stimulation. Curr. Opin. Neurol. 32, 511–520. https://doi.org/10.1097/WCO.0000000000000679.

Horn, A., Blankenburg, F., 2016. Toward a standardized structural-functional group connectome in MNI space. NeuroImage 124, 310–322. https://doi.org/10.1016/j.neuroimage.2015.08.048.

Horn, A., Fox, M.D., 2020. Opportunities of connectomic neuromodulation. NeuroImage 221, 117180. https://doi.org/10.1016/j.neuroimage.2020.117180.

Horn, A., Kühn, A.A., 2015. Lead-DBS: a toolbox for deep brain stimulation electrode localizations and visualizations. NeuroImage 107, 127–135. https://doi.org/10.1016/j.neuroimage.2014.12.002.

Horn, A., Ostwald, D., Reisert, M., Blankenburg, F., 2014. The structural-functional connectome and the default mode network of the human brain. NeuroImage 102 (Pt 1), 142–151. https://doi.org/10.1016/j.neuroimage.2013.09.069.

Horn, A., Reich, M., Vorwerk, J., Li, N., Wenzel, G., Fang, Q., Schmitz-Hubsch, T., Nickl, R., Kupsch, A., Volkmann, J., Kühn, A.A., Fox, M.D., 2017. Connectivity predicts deep brain stimulation outcome in Parkinson disease. Ann. Neurol. 82, 67–78. https://doi.org/10.1002/ana.24974.

Horn, A., Li, N., Dembek, T.A., Kappel, A., Boulay, C., Ewert, S., Tietze, A., Husch, A., Perera, T., Neumann, W.-J., Reisert, M., Si, H., Oostenveld, R., Rorden, C., Yeh, F.-C., Fang, Q., Herrington, T.M., Vorwerk, J., Kühn, A.A., 2019a. Lead-DBS v2: towards a comprehensive pipeline for deep brain stimulation imaging. NeuroImage 184, 293–316. https://doi.org/10.1016/j.neuroimage.2018.08.068.

Horn, A., Wenzel, G., Irmen, F., Hübl, J., Li, N., Neumann, W.-J., Krause, P., Bohner, G., Scheel, M., Kühn, A.A., 2019b. Modulating the human functional connectome using deep brain stimulation (preprint). Neuroscience. https://doi.org/10.1101/537712.

Howell, B., McIntyre, C.C., 2016. Analyzing the tradeoff between electrical complexity and accuracy in patient-specific computational models of deep brain stimulation. J. Neural Eng. 13, 036023 https://doi.org/10.1088/1741-2560/13/3/036023.

Howell, B., McIntyre, C.C., 2017. Role of soft-tissue heterogeneity in computational models of deep brain stimulation. Brain Stimulat. 10, 46–50. https://doi.org/10.1016/j.brs.2016.09.001.

Irmen, F., Horn, A., Mosley, P., Perry, A., Petry-Schmelzer, J.N., Dafsari, H.S., Barbe, M., Visser-Vandewalle, V., Schneider, G.-H., Li, N., Kübler, D., Wenzel, G., Kühn, A., 2020. Left prefrontal impact links subthalamic stimulation with depressive symptoms. Ann. Neurol. https://doi.org/10.1002/ana.25734.

Johnson, G.A., Calabrese, E., Badea, A., Paxinos, G., Watson, C., 2012. A multidimensional magnetic resonance histology atlas of the Wistar rat brain. NeuroImage 62, 1848–1856. https://doi.org/10.1016/j.neuroimage.2012.05.041.

Kastner, D.B., Kharazia, V., Nevers, R., Smyth, C., Astudillo-Maya, D.A., Williams, G.M., Yang, Z., Holobetz, C.M., Santina, L.D., Parkinson, D.Y., Frank, L.M., 2020. Scalable method for micro-CT analysis enables large scale quantitative characterization of brain lesions and implants. Sci. Rep. 10, 20851. https://doi.org/10.1038/s41598-020-77796-3.

Khan, A.M., Perez, J.G., Wells, C.E., Fuentes, O., 2018. Computer vision evidence supporting Craniometric alignment of rat brain atlases to streamline expert-guided, first-order migration of hypothalamic spatial datasets related to behavioral control. Front. Syst. Neurosci. 12, 7. https://doi.org/10.3389/fnsys.2018.00007.

Király, B., Balázsfi, D., Horváth, I., Solari, N., Sviatkó, K., Lengyel, K., Birtalan, E., Babos, M., Bagaméry, G., Máthé, D., Szigeti, K., Hangya, B., 2020. In vivo localization of chronically implanted electrodes and optic fibers in mice. Nat. Commun. 11, 4686. https://doi.org/10.1038/s41467-020-18472-y.

Krauss, J.K., Lipsman, N., Aziz, T., Boutet, A., Brown, P., Chang, J.W., Davidson, B., Grill, W.M., Hariz, M.I., Horn, A., Schulder, M., Mammis, A., Tass, P.A., Volkmann, J., Lozano, A.M., 2020. Technology of deep brain stimulation: current status and future directions. Nat. Publ. Group 1–13. https://doi.org/10.1038/s41582-020-00426-z.

Kühn, A.A., Williams, D., Kupsch, A., Limousin, P., Hariz, M., Schneider, G.-H., Yarrow, K., Brown, P., 2004. Event-related beta desynchronization in human subthalamic nucleus correlates with motor performance, 127, pp. 735–746. https://doi.org/10.1093/brain/awh106.

Kupsch, A., Benecke, R., Müller, J., Trottenberg, T., Schneider, G.-H., Poewe, W., Eisner, W., Wolters, A., Müller, J.-U., Deuschl, G., Pinsker, M.O., Skogseid, I.M., Roeste, G.K., Vollmer-Haase, J., Brentrup, A., Krause, M., Tronnier, V., Schnitzler, A., Voges, J., Nikkhah, G., Vesper, J., Naumann, M., Volkmann, J., Deep-Brain Stimulation for Dystonia Study Group, 2006. Pallidal deep-brain stimulation in primary generalized or segmental dystonia. N. Engl. J. Med. 355, 1978–1990. https://doi.org/10.1056/NEJMoa063618.

Li, N., Baldermann, J.C., Kibleur, A., Treu, S., Akram, H., Elias, G.J.B., Boutet, A., Lozano, A.M., Al-Fatly, B., Strange, B., Barcia, J.A., Zrinzo, L., Joyce, E., Chabardes, S., Visser-Vandewalle, V., Polosan, M., Kuhn, J., Kühn, A.A., Horn, A., 2020. A unified connectomic target for deep brain stimulation in obsessive-compulsive disorder. Nat. Commun. 11, 3364. https://doi.org/10.1038/s41467-020-16734-3.

Li, N., Hollunder, B., Baldermann, J.C., Kibleur, A., Treu, S., Akram, H., Al-Fatly, B., Strange, B., Barcia, J.A., Zrinzo, L., Joyce, E., Chabardes, S., Visser-Vandewalle, V., Polosan, M., Kuhn, J., Kühn, A.A., Horn, A., 2021. A unified functional network target for deep brain stimulation in obsessive-compulsive disorder. Biol. Psychiatry 0. https://doi.org/10.1016/j.biopsych.2021.04.006.

Masís, J., Mankus, D., Wolff, S.B.E., Guitchounts, G., Joesch, M., Cox, D.D., 2018. A micro-CT-based method for quantitative brain lesion characterization and electrode localization. Sci. Rep. 8, 5184. https://doi.org/10.1038/s41598-018-23247-z.

McIntyre, C.C., Richardson, A.G., Grill, W.M., 2002. Modeling the excitability of mammalian nerve fibers: influence of Afterpotentials on the recovery cycle. J. Neurophysiol. 87, 995–1006. https://doi.org/10.1152/jn.00353.2001.

Miocinovic, S., Noecker, A.M., Maks, C.B., Butson, C.R., McIntyre, C.C., 2007. Cicerone: stereotactic neurophysiological recording and deep brain stimulation electrode placement software system. Acta Neurochir. Suppl. 97, 561–567.

Neumann, W.-J., Kühn, A.A., 2017. Subthalamic beta power-Unified Parkinson's disease rating scale III correlations require akinetic symptoms. Mov. Disord. 32, 175–176. https://doi.org/10.1002/mds.26858.

Papp, E.A., Leergaard, T.B., Calabrese, E., Johnson, G.A., Bjaalie, J.G., 2014. Waxholm space atlas of the Sprague Dawley rat brain. NeuroImage 97, 374–386. https://doi.org/10.1016/j.neuroimage.2014.04.001.

Paxinos, G., Watson, C., 2007. The Rat Brain in Stereotaxic Coordinates, 6th ed. Academic Press/Elsevier, Amsterdam, Boston.

Pieper, S., Halle, M., Kikinis, R., 2004. 3D Slicer. In: 2004 2nd IEEE International Symposium on Biomedical Imaging: Macro to Nano (IEEE Cat No. 04EX821). Presented at the 2004 2nd IEEE International Symposium on Biomedical Imaging: Macro to Nano. IEEE, Arlington, VA, USA, pp. 632–635. https://doi.org/10.1109/ISBI.2004.1398617.

Pieper, S., Lorensen, B., Schroeder, W., Kikinis, R., 2006. The NA-MIC Kit: ITK, VTK, Pipelines, Grids and 3D Slicer as An Open Platform for the Medical Image Computing Community. In: 3rd IEEE International Symposium on Biomedical Imaging: Macro to Nano, 2006. Presented at the 3rd IEEE International Symposium on Biomedical Imaging: Macro to Nano, 2006. IEEE, Arlington, Virginia, USA, pp. 698–701. https://doi.org/10.1109/ISBI.2006.1625012.

Rangarajan, J.R., Vande Velde, G., van Gent, F., De Vloo, P., Dresselaers, T., Depypere, M., van Kuyck, K., Nuttin, B., Himmelreich, U., Maes, F., 2016. Image-based in vivo assessment of targeting accuracy of stereotactic brain surgery in experimental rodent models. Sci. Rep. 6, 38058. https://doi.org/10.1038/srep38058.

Ribes, A., Caremoli, C., 2007. Salome platform component model for numerical simulation. In: 31st Annual International Computer Software and Applications Conference - Vol. 2 - (COMPSAC 2007). Presented at the 31st Annual International Computer Software and Applications Conference - Vol. 2 - (COMPSAC 2007). IEEE, Beijing, China, pp. 553–564. https://doi.org/10.1109/COMPSAC.2007.185.

Sanders, T.H., Jaeger, D., 2016. Optogenetic stimulation of cortico-subthalamic projections is sufficient to ameliorate bradykinesia in 6-ohda lesioned mice. Neurobiol. Dis. 95, 225–237. https://doi.org/10.1016/j.nbd.2016.07.021.

Schmidt, C., van Rienen, U., 2012. Modeling the field distribution in deep brain stimulation: the influence of anisotropy of brain tissue. IEEE Trans. Biomed. Eng. 59, 1583–1592. https://doi.org/10.1109/TBME.2012.2189885.

Schmidt, C., Dunn, E., Lowery, M., van Rienen, U., 2018. Uncertainty quantification of oscillation suppression during DBS in a coupled finite element and network model.

IEEE Trans. Neural Syst. Rehabil. Eng. 26, 281–290. https://doi.org/10.1109/TNSRE.2016.2608925.

Sridhar, K., Evers, J., Botelho, D.P., Lowery, M.M., 2019. Estimation of dispersive properties of encapsulation tissue surrounding deep brain stimulation electrodes in the rat. In: 2019 41st Annual International Conference of the IEEE Engineering in Medicine and Biology Society (EMBC). Presented at the 2019 41st Annual International Conference of the IEEE Engineering in Medicine & Biology Society (EMBC). IEEE, Berlin, Germany, pp. 2973–2976. https://doi.org/10.1109/EMBC.2019.8857062.

Swanson, L.W. (Ed.), 1998. Brain maps: structure of the rat brain; a laboratory guide with printed and electronic templates for data, models, and schematics, 2. rev. ed. Elsevier, Amsterdam.

Treu, S., Strange, B., Oxenford, S., Kühn, A., Li, N., Horn, A., 2020. Deep Brain Stimulation: Imaging on a group level. bioRxiv 142. https://doi.org/10.1101/2020.01.14.904615, 3086–47.

Vedam-Mai, V., Deisseroth, K., Giordano, J., Lazaro-Munoz, G., Chiong, W., Suthana, N., Langevin, J.-P., Gill, J., Goodman, W., Provenza, N.R., Halpern, C.H., Shivacharan, R.S., Cunningham, T.N., Sheth, S.A., Pouratian, N., Scangos, K.W., Mayberg, H.S., Horn, A., Johnson, K.A., Butson, C.R., Gilron, R., de Hemptinne, C., Wilt, R., Yaroshinsky, M., Little, S., Starr, P., Worrell, G., Shirvalkar, P., Chang, E., Volkmann, J., Muthuraman, M., Groppa, S., Kühn, A.A., Li, L., Johnson, M., Otto, K. J., Raike, R., Goetz, S., Wu, C., Silburn, P., Cheeran, B., Pathak, Y.J., Malekmohammadi, M., Gunduz, A., Wong, J.K., Cernera, S., Wagle Shukla, A., Ramirez-Zamora, A., Deeb, W., Patterson, A., Foote, K.D., Okun, M.S., 2021. Proceedings of the eighth annual deep brain stimulation think tank: advances in optogenetics, ethical issues affecting DBS research, neuromodulatory approaches for depression, adaptive neurostimulation, and emerging DBS technologies. Front. Hum. Neurosci. 15 https://doi.org/10.3389/fnhum.2021.644593.

Yelnik, J., Damier, P., Demeret, S., Gervais, D., Bardinet, E., Bejjani, B.-P., François, C., Houeto, J.-L., Arnule, I., Dormont, D., Galanaud, D., Pidoux, B., Cornu, P., Agid, Y., 2003. Localization of stimulating electrodes in patients with Parkinson disease by using a three-dimensional atlas-magnetic resonance imaging coregistration method. J. Neurosurg. 99, 89–99. https://doi.org/10.3171/jns.2003.99.1.0089.

Zhao, S., Li, G., Tong, C., Chen, W., Wang, P., Dai, J., Fu, X., Xu, Z., Liu, X., Lu, L., Liang, Z., Duan, X., 2020. Full activation pattern mapping by simultaneous deep brain stimulation and fMRI with graphene fiber electrodes. Nat. Commun. 11, 1788. https://doi.org/10.1038/s41467-020-15570-9.